Optical Materials 75 (2018) 297–303

Contents lists available at ScienceDirect

Optical Materials

journal homepage: www.elsevier.com/locate/optmat

Luminescent Eu^{3+} doped $Al_6Ge_2O_{13}$ crystalline compounds obtained by the sol gel process for photonics

Lauro J.Q. Maia [a, *], Fausto M. Faria Filho [a], Rogéria R. Gonçalves [b], Sidney J.L. Ribeiro [c]

[a] Grupo Física de Materiais, Instituto de Física, Campus II, CP 131, 74001-970, Universidade Federal de Goiás-UFG, Goiânia, GO, Brazil
[b] Departamento de Química, Faculdade de Filosofia, Ciências e Letras de Ribeirão Preto, Av. Bandeirantes 3900, 14040-901, Universidade de São Paulo-USP, Ribeirão Preto, SP, Brazil
[c] Institute of Chemistry, CP 355, 14801-970, São Paulo State University-UNESP, Araraquara, SP, Brazil

ARTICLE INFO

Article history:
Received 21 July 2017
Received in revised form
27 September 2017
Accepted 23 October 2017
Available online 6 November 2017

Keywords:
$Al_6Ge_2O_{13}$ crystalline phase
Eu^{3+} doped
Structural properties
Optical properties

ABSTRACT

We synthesized pure and Eu^{3+} doped $Al_6Ge_2O_{13}$ samples by an easy and low-cost sol-gel route using the GeO_2, $Al(NO_3)_3 \cdot 9H_2O$ and $Eu(NO3)_3 \cdot 6H_2O$ as precursors, tetramethylammonium hydroxide and ethanol as solvents. The $Al_6Ge_2O_{13}$ crystalline phase possesses orthorhombic structure and is a potential host for rare earth ions, especially due to high aluminum concentration. Homogeneous and transparent sols and gels were obtained. The samples containing 1 mol% of Eu^{3+} were heat-treated at 1000 °C to eliminate organic compounds, providing high optical quality and structural purity. All materials were characterized by thermogravimetric and differential thermal analysis, X-ray diffraction, Fourier transform infrared spectroscopy, high resolution transmission electron microscopy, selected area electron diffraction, diffuse reflectance spectra in the ultraviolet–visible–near infrared regions and photoluminescence measurements. High purity of Eu^{3+} doped $Al_6Ge_2O_{13}$ orthorhombic phase and well crystallized grain dimensions of around 100 nm was obtained with high red photoluminescence emission. The decay lifetime of $^5D_0$ level from Eu^{3+} (the emission at 612 nm) was determined, being between 0.97 and 2.12 ms, and an average quantum efficiency of 54% was determined (considering the average experimental lifetime of 1.77 ms). Moreover, it was calculated and analyzed some parameters of Judd-Ofelt theory applied to Eu^{3+} emissions from $Al_6Ge_2O_{13}$ host. The results show that Eu^{3+} doped $Al_6Ge_2O_{13}$ crystalline compounds have large potential to be used in displays and LED devices.

1. Introduction

Scientific community has great interest in rare earth ions doped inorganic materials due to their interesting optical properties. Rare earth doped inorganic materials have been used in solid-state lasers, active planar waveguides, optical fiber amplifiers, lighting emitting diodes (LED's), memories, solar cells, and displays [1–3]. Rare-earth (RE) trivalent ions can emit light from the near-infrared (NIR) to the ultraviolet (UV) due to intra-4*f* or internal 4*f*–5*d* transitions [1].

Europium ions (Eu^{3+}) have interesting optical features such as well-defined spectral lines and red/orange emissions, which have been exploited for technological applications in displays, fluorescent lamps, fluoroimmunoassays. The most standard commercial red phosphors are based on Eu^{3+} doped oxides (Y_2O_3:Eu^{3+}, YPO_4:Eu^{3+}, YVO_4:Eu^{3+}, $Y_2(WO_4)_3$:Eu^{3+}, Y_2O_2S:Eu^{3+}). In order to make red phosphor with high red emission intensity, a high europium concentration is required. However, due to the onset of concentration quenching in commercial matrices, the relatively low efficiency can be achieved with high concentrations of Eu^{3+}. On the other hand, the Eu^{3+} ion is often used as structural probe when doped in crystalline or amorphous structure due to its particular optical transitions [4], and a detailed understanding of the local structure and bonding of dopant ions is important for optical device engineering [5].

Concerning improvement of optical properties, firstly a reduction or elimination of non-radiative processes is required, such as OH groups which are responsible for luminescence quenching. Multiphonon relaxation represents one significant non-radiative process and, consequently, the choice and control of vibrational structure of the host is crucial to enhance the radiative process. Other important parameter is related to rare earth concentration

* Corresponding author.
E-mail address: lauro@ufg.br (L.J.Q. Maia).

https://doi.org/10.1016/j.optmat.2017.10.038
0925-3467/

and their distribution in the host, where ion-ion interactions give rise to non-radiative processes as energy migration, cross relaxation, which reduce considerably the luminescence [6,7]. Besides, optical features improvement can be also achieved changing the microenvironment of the rare earth ions, defined by symmetry sites and refractive index, which influences the transitions probabilities. Therefore, there is a great interest to develop physically and chemically stable host matrices with high rare-earth ions solubility, especially for europium to have pure red emissions to be used in LED and display devices.

One potential rare earth host candidate is the $Al_6Ge_2O_{13}$ crystalline phase, which is characterized by an orthorhombic structure containing high concentration of aluminum ions, which can allow noteworthy rare earth content incorporation to be used in solid-state lasers, optical amplifiers, LED's, and displays.

Nevertheless, the literature reports that obtaining $Al_6Ge_2O_{13}$ crystalline phase is difficult because high temperatures are required, as high as 1325 °C, and long heat-treatment periods (15 h), especially by solid state reaction [8–10] using $Al(NO_3)_3{\cdot}9H_2O$ or Al_2O_3 as precursors for aluminum and GeO_2 for germanium. Important to stress that the traditional sol-gel route, which is a soft route, has been used for producing homogeneously different samples using alkoxydes, mainly TEOG [$Ge(OC_2H_5)_4$] as a germanium precursor [11–13]. However, germanium alkoxydes are very expensive and highly sensitive to atmospheric humidity, requiring its manipulation in a dry glove box. To overcome this inconvenience, we have developed in recent works [1,14] a methodology, which doesn't require the use of controlled atmosphere and humidity. Recently, Er^{3+} doped SiO_2-Al_2O_3-GeO_2 compounds were prepared and $Al_6Ge_2O_{13}$ nanocrystallites were obtained around 1000 °C [1].

In the present work, we synthesized pure and Eu^{3+} doped $Al_6Ge_2O_{13}$ samples by simple and lower cost sol-gel route than traditional procedures. The structural, microstructural and spectroscopic properties of the pure and Eu^{3+} doped $Al_6Ge_2O_{13}$ compounds were studied to be used in displays and LED's as red emitters.

2. Experimental procedure

2.1. Synthesis

Transparent sols were prepared by the sol-gel route to form the polymeric precursor. First, citric acid (CA, $C_6H_8O_7$, 99.5% purity, Synth) was diluted in ethanol (EtOH, C_2H_5OH, 99.5% purity, Chemycalis) for 30 min under vigorous stirring (solution 1). $Al(NO_3)_3{\cdot}9H_2O$ (aluminum nitrate nonahydrate, 98% purity, Sigma Aldrich) and $Eu(NO_3)_3{\cdot}5H_2O$ (europium nitrate pentahydrate, 99.9% purity, Sigma Aldrich) were diluted in ethanol separately (solution 2). In parallel, 200 mg of GeO_2 (germanium oxide, 99.998% purity, Sigma Aldrich) was reacted with 3 ml of TMAH solution (tetramethylammonium hydroxide, $C_4H_{13}NO$, 25% volume in water, Sigma Aldrich) and 200 ml of deionized H_2O, and stirred vigorously for 20 min to obtain the solution 3. Solution 3 was added to the solution 1, followed by solution 2 addition. The final solution was vigorously stirred for 20 min and remained resting at room temperature for 24 h, yielding stable and transparent sols. The molar ratio of the citric acid and metal was 3:1, and each 1 g of CA was dissolved in 2 ml of EtOH, and each 1 g of aluminum and europium nitrates was dissolved in 10 ml of EtOH.

To eliminate the solvent and trigger gelation (hydrolysis and condensation reactions), the sols were oven-dried at 150 °C for 24 h. The dry gels were then calcined at 400 °C for 24 h. Each sample was ground into fine powder in an agate mortar and heat-treated at 1000 °C. The heat treatments were performed in a muffle furnace under air atmosphere for 1 h, using alumina crucibles.

2.2. Characterization

The thermal decomposition and crystallization processes of the powders previously calcined at 400 °C/24 h were studied by the thermogravimetric (TGA) and differential thermal analyses (DTA) (Setaram LABSYS EVO), which were performed simultaneously under a continuous flow of O_2. Samples (~20 mg) were heated in a platinum crucible at 10 °C/min from 25 °C to 1150 °C, and a platinum crucible was used as reference during the measurements.

After annealing at 1000 °C, the samples were characterized structurally by X-ray diffraction (XRD) and Fourier transform infrared spectroscopy (FTIR). The XRD measurements were taken with a Shimadzu XRD-6000 X-ray diffractometer with Bragg-Brentano theta-2 theta geometry, at a continuous scan speed of 0.04°/s from 15 to 65°. $K\alpha$ radiation of 1.54059 Å from a Cu tube operating at 40 kV was used. The FTIR measurements were obtained with a Perkin Elmer Spectrum 400 FT-IR spectrometer. The experiments were performed from 4000 to 400 cm^{-1} with a resolution of 2 cm^{-1}, and 56 spectra were recorded.

High-resolution transmission electron microscope (HRTEM) was used for obtaining images from a JEOL JEM 2010 operating at 200 keV, and electron diffraction (SAED) patterns from selected area.

The diffuse reflectance spectra were obtained using a UV–Vis–NIR PerkinElmer Lambda 1200WB spectrophotometer and a Praying Mantis® accessory. The $BaSO_4$ powder from Sigma-Aldrich was used as standard reflectance material.

The photoluminescence (PL) emission spectra were performed at room temperature using a Horiba-Jobin Yvon Fluorolog FL3-221 spectrofluorimeter, equipped with double monochromator and a Hamamatsu photomultiplier tube. For excitation, a continuous 450 W Xe arc lamp was employed. PL emission spectra were corrected for the spectral response of the monochromators and the detector using a typical correction spectrum provided by the manufacturer. The PL decay curves at 612 nm were obtained under excitation at 394 nm using a pulsed Xe lamp (3 μs bandwidth) in a Horiba-Jobin Yvon Fluorolog FL3-222 spectrofluorimeter.

3. Results and discussion

Fig. 1 shows the TG and DTA curves of Eu^{3+} doped $Al_6Ge_2O_{13}$ compound previously calcined at 400 °C. Although the technique is

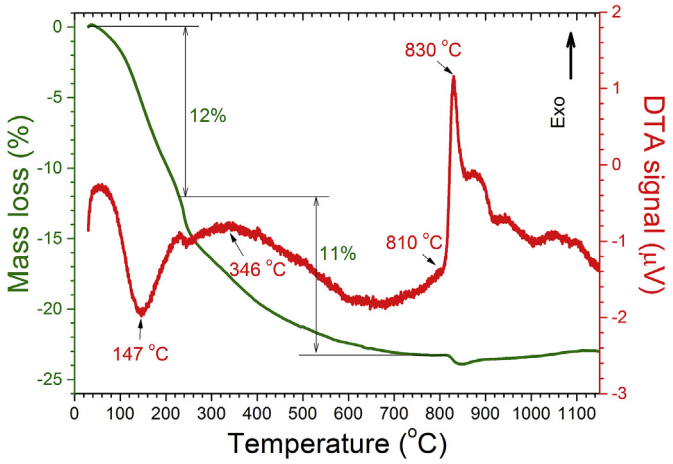

Fig. 1. TG and DSC curves of the Eu^{3+} doped $Al_6Ge_2O_{13}$ compound previously calcined at 400 °C.

semi-quantitative, mass variation can be measured accurately. The TG curves revealed mass loss events, which were related to endothermic or exothermic reactions as indicated by the DTA curves. These endothermic or exothermic reactions are attributed to three main reactions: firstly, elimination of adsorbed water (peak around 147 °C) with a mass loss of 12%; secondly, carbon oxidation and its elimination in the form of CO and CO_2 (combustion reaction, broad peak centered at 346 °C) with a mass loss of 11%; and finally, a crystallization process starting at 810 °C, with the peak at 830 °C, which is assigned to the $Al_6Ge_2O_{13}$ crystalline phase formation. In the crystallization process, the mass of the sample reduces around 1% was related to an elimination of carbon and/or hydroxyl groups strongly linked to the metals, followed by a gradual increasing of the mass probably due to oxygen absorption from atmosphere (residual oxidation reaction) and some broad exothermic peaks related to changes in the AlO_4 e AlO_6 groups ratio in the crystalline phase (to be confirmed in future works for this phase). Some works on mullite ($3Al_2O_3$:$2SiO_2$) studies mention that the relation between tetrahedral and octahedral groups is dependent of annealing temperature [15].

Fig. 2 shows XRD patterns of pure and Eu^{3+} doped samples heat-treated at 1000 °C. For comparison, the diffraction position from the JCPDS card number 71-1061 was included in Fig. 2. Only the $Al_6Ge_2O_{13}$ phase in an orthorhombic structure and the *Pbam* (55) space group (mullite-type structure) crystallized at 1000 °C. Based on the XRD data displayed in Fig. 2 (peak position and Miller index of diffracted planes), and using the *Rede 93* software program developed by Paiva Santos et al. [16], the following cell parameters were calculated: $a = 7.61(2)$ Å, $b = 7.97(8)$ Å, and $c = 2.93(4)$ Å for pure sample and $a = 7.66(2)$ Å, $b = 7.80(5)$ Å, and $c = 2.91(3)$ Å for Eu^{3+} doped sample. These values are similar to those listed on JCPDS card number 71-1061 ($a = 7.65(2)$ Å, $b = 7.779(2)$ Å, $c = 2.925(2)$ Å). The cell volume was 178(5) $Å^3$ for pure, was 174(3) $Å^3$ for Eu^{3+} doped, both similar to JCPDS card number 71-1061 with 174.06(6) $Å^3$. Comparison with pure $Al_6Ge_2O_{13}$ and JCPDS reference suggests that the insertion of rare earth ions don't change significantly the cell volume and parameters. Gao et al. [17] produced $Al_6Ge_2O_{13}$ ceramic powder by the co-precipitation method, using $Al(NO_3)_3$ and $Cl_3GeCH_2CH_2COOH$ as precursors. In comparison with reported synthesis, pure and Eu^{3+} doped $Al_6Ge_2O_{13}$ phase at 1000 °C were easily obtained using a friendly chemical route.

The $Al_6Ge_2O_{13}$ phase in an orthorhombic structure have the same *Pbam* (55) space group of mullite structure, as a consequence it has been assumed that both compounds has comparable structures and consequently Ge^{4+} are distributed in the sites occupied by Si^{4+}. The backbone of the mullite structure is edge-sharing AlO_6 octahedra (designated as M sites) forming chains running parallel to the crystallographic *c*-axis [18]. A part of the Si^{4+} is replaced by Al^{3+}. The compensation of the substitution-induced charge deficiency is achieved by removal of a number of oxygen atoms bridging the tetrahedral T_2O_5 groups [designated as O3 or alternatively O(C)]. This produces oxygen vacancies (designated as O3 or O vacancies), according to the coupled substitution $2Si^{4+} + O^{2-} \rightarrow 2Al^{3+} +$ vacancy (□), with x of the general formula related to the number of oxygen vacancies per unit cell in the composition range $0 < x < 0.67$. The formation of O vacancies is accompanied by the displacement of the T positions close to the bridging O atoms to the new T* positions. The T^*O_4 tetrahedra form trimers or triclusters of three tetrahedral having a common bridging O atom. The studies mentioned that most of the T* sites are occupied by Al. The combination of octahedral chains with tetrahedral di and triclusters and O vacancies produces disturbed structural channels running parallel to the crystallographic *c*-axis. The distribution of the O vacancies and of the tetrahedral Al and Si atoms in a first approach appears random [18]. Aryal et al. [19] shown that mullite is an example of 2 x 2 x 2 supercell. All fully occupied sites were retained and those with partial occupations had the appropriate number of atoms removed. Oxygen vacancies were created by removing some O atoms that were close to such that the supercell was stoichiometric and charge neutral. The resulting 126-atom supercell for mullite consists of 36 Al, 12 Si, and 78 O atoms [20], being ~16 units of AlO_6 octahedra and ~20 units of AlO_4 tetrahedra. However, the tetrahedral to octahedral aluminum site ratio is dependent on the heat-treatment temperature [15] and certainly on the synthesis process.

The solubility of Eu^{3+} in $Al_6Ge_2O_{13}$ orthorhombic structure is not known, but can be strongly limited by the aluminum sites quantity. Note that Ge^{4+}, Al^{3+} and Eu^{3+} have ionic radius of 0.39, 0.535, and 0.947 Å respectively [20]. As a consequence, it can be assumed that Eu^{3+} should prefer replace Al^{3+} of AlO_6 octahedra (designated as M sites), because they have same valence and smaller difference between its ionic radius, also the octahedral sites can accommodate easily lanthanide elements than tetrahedral sites. Note that in octahedral sites of mullite the average interatomic distance between Al and O atoms is 1.913(2) Å, and in tetrahedral sites is 1.700(2) Å [15], and consequently some octahedral sites can well accommodate Eu^{3+} ions.

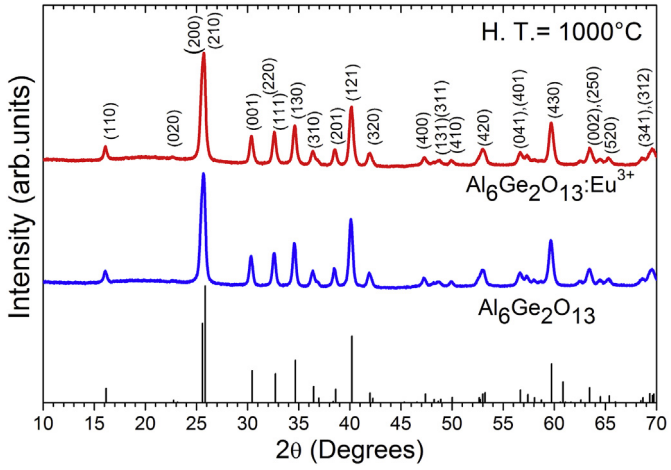

Fig. 2. X-ray diffraction patterns of pure and Eu^{3+} doped $Al_6Ge_2O_{13}$ heat treated at 1000 °C, and the diffraction pattern of the JCPDS card number 71-1061 for comparison.

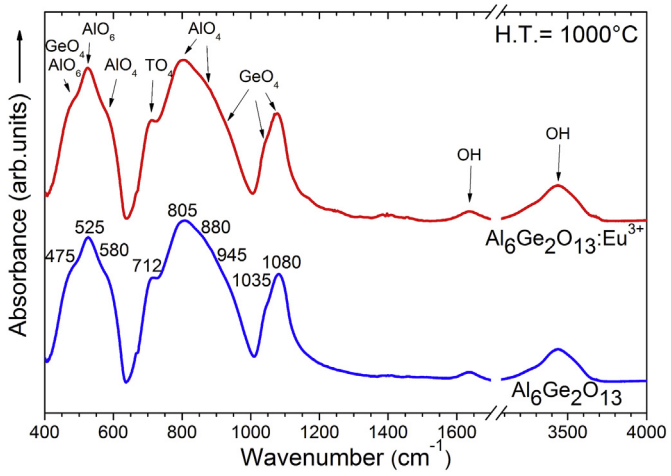

Fig. 3. Vibrational absorption spectra in the infrared region of pure and Eu^{3+} doped $Al_6Ge_2O_{13}$ powders heat treated at 1000 °C.

Fig. 3 shows the FTIR spectra of pure and Eu^{3+} doped samples heat-treated at 1000 °C. Absorption band attributed to stretching vibrational mode of hydroxyl groups (OH) at around 1639 and 3450 cm^{-1} were observed in both samples. Low intensity suggests significant elimination of OH content without relevant change in the presence of Eu^{3+} ions.

The bands in the region of 400–1200 cm^{-1}, centered at 475, 525, 580, 712, 805, 880, 945, 1035, and 1080 cm^{-1} correspond to vibrational modes of AlO_4, AlO_6 and GeO_4 groups of the $Al_6Ge_2O_{13}$ crystals, as illustrated in Fig. 3. Their assignments are listed in Table 1, and are in accordance with those assigned to the vibrational modes of the $Al_6Ge_2O_{13}$ crystalline phase reported by Meinhold and Mackenzie [10].

Fig. 4(a) and (c) shows HRTEM images of pure and Eu^{3+} doped $Al_6Ge_2O_{13}$ samples, respectively. Well defined atomic planes of 0.34(3) nm was observed in pure sample and attributed to the (210) plane of the orthorhombic $Al_6Ge_2O_{13}$ phase, and 0.53(3) nm assigned to the (110) plane in Eu^{3+} doped sample, in agreement with crystallization of the $Al_6Ge_2O_{13}$ phase. The SAED patterns in Fig. 4(b) and (d) reveal that the particles are monocrystals.

Band gap values were calculated from the diffuse reflectance measurements displayed in Fig. 5(a) and (b), using the procedure previously described by Pessoni and co-workers [21]. In the Kubelka-Munk model [22], the remission function $F(R_\infty)$ is defined as:

$$F(R_\infty) = \frac{(1 - R_\infty)^2}{2R_\infty} \quad (1)$$

where R_∞ is the measured reflectance in % normalized by a standard, which in our case was $BaSO_4$. The band gap (E_g) and the absorption coefficient (α) are correlated by $\alpha h\nu = C_1\sqrt{h\nu - E_g}$, where $h\nu$ is the photon energy and C_1 is a proportionality constant. The remission function can be written by:

$$[F(R_\infty)h\nu]^2 = C_2(h\nu - E_g) \quad (2)$$

Therefore, using $C_2 = 1$, E_g is obtained from the linear fit of $[F(R_\infty)h\nu]^2$ versus $h\nu$.

In Fig. 5(a) and (b) a high reflectivity can be seen from 350 nm up to 800 nm for both compounds, attesting the optical quality of the pure and Eu^{3+} doped $Al_6Ge_2O_{13}$ crystalline powders. The decrease of the reflectance intensity starts ~350 nm and finishes ~250 nm wavelengths. Two low absorption peaks around 395 nm and 460 were attributed to Eu^{3+} due to $^7F_0 \rightarrow {}^5L_6$ and $^7F_0 \rightarrow {}^5D_2$ transitions, as indicated in Fig. 5(b). The insets in Fig. 5(a) and (b) shows the $[F(R_\infty)h\nu]^2$ vs. $h\nu$ curves with linear fitting at higher energies. The optical band gap energy (E_g) is the intercept of the fitting with the horizontal line $[F(R_\infty)h\nu]^2 = 0$. The determined E_g were 4.24(5) eV for pure sample and 4.30(5) eV for Eu^{3+} doped sample. Both samples can be considered non-conducting.

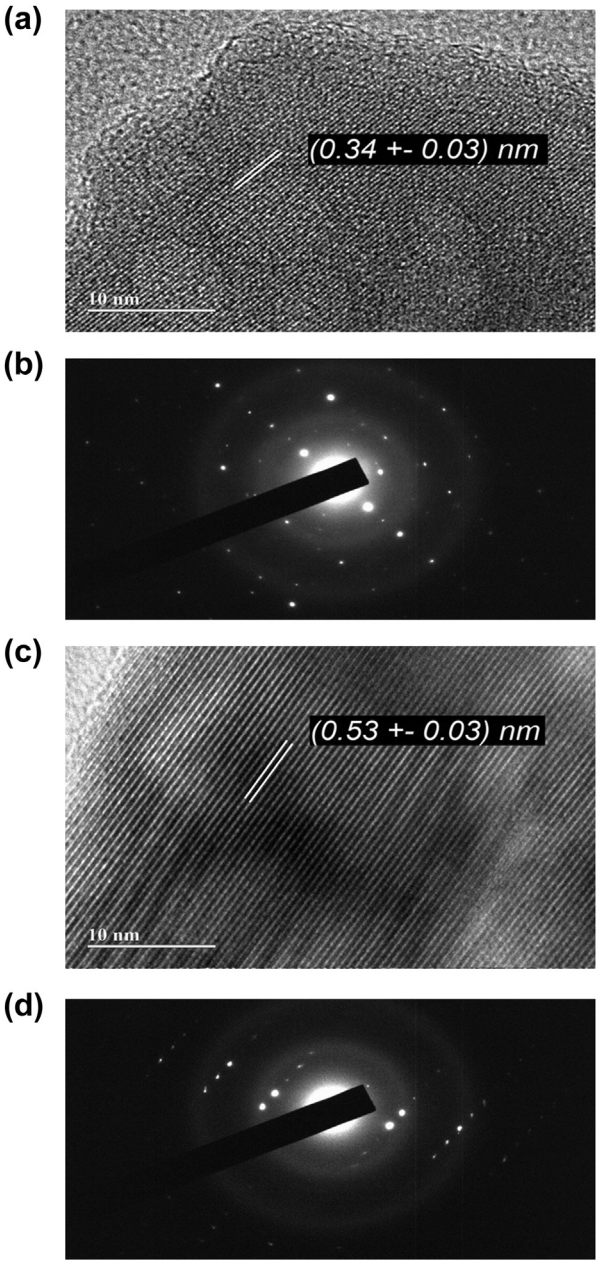

Fig. 4. (a) and (c) HRTEM images and (b) and (d) SAED of pure and Eu^{3+} doped $Al_6Ge_2O_{13}$ heat treated at 1000 °C, respectively.

Fig. 6 shows the excitation and emission PL spectra of pure and Eu^{3+} doped $Al_6Ge_2O_{13}$ crystalline powders. Pure $Al_6Ge_2O_{13}$ shows a

Table 1
Frequency of vibrational modes from spectra in Fig. 2 for both samples in comparison to those from Refs. [9,10].

	Pure $Al_6Ge_2O_{13}$ (This work)	Eu^{3+} doped $Al_6Ge_2O_{13}$ (This work)	From Ref. [9]	From Ref. [10]	Assignments
Frequency (cm^{-1})	475	475	469		O-Ge-O bend and Al-*O*-Al bend
	525	525	541	510	Al-O stretch
	580	580	593		O-Al-O bend
	712	712	709	660	T-*O*-T bend, in-plane T is Ge or Al
	805	805	779	792	Al-O stretch, in-plane
	880	880	831		Al-O strect, out-of-plane
	945	945	889		Ge-O stretch, out-of-plane
	1035	1035	1035		Ge-O stretch, in-plane
	1080	1080	1068	1077	Ge-O stretch, in-plane

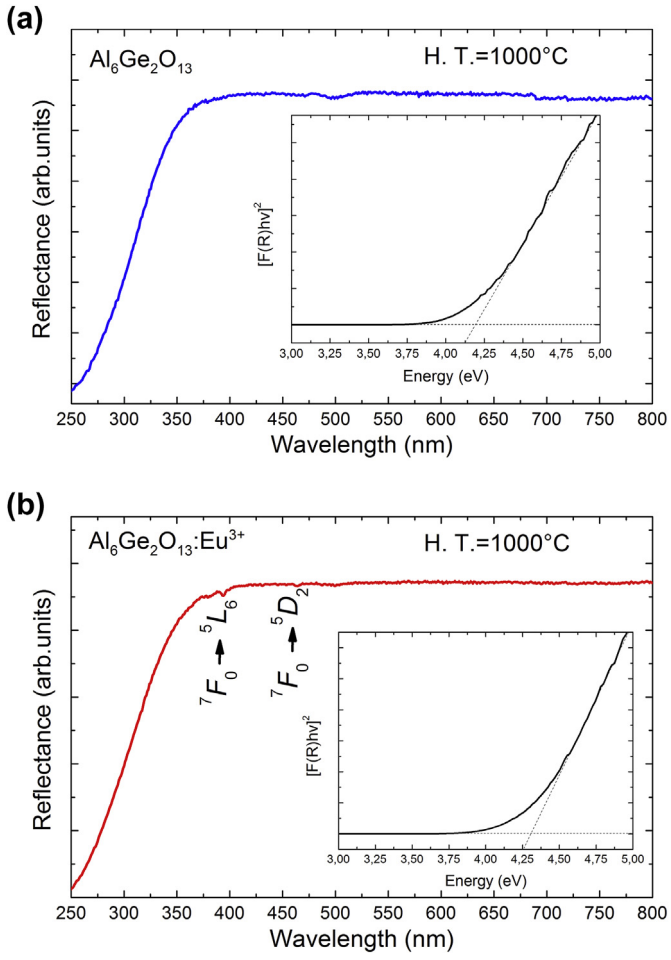

Fig. 5. Room temperature diffuse reflectance of (a) pure and (b) Eu^{3+} doped $Al_6Ge_2O_{13}$ crystalline powders. Inset is the bandgap (Eg) determined by diffuse reflectance curves.

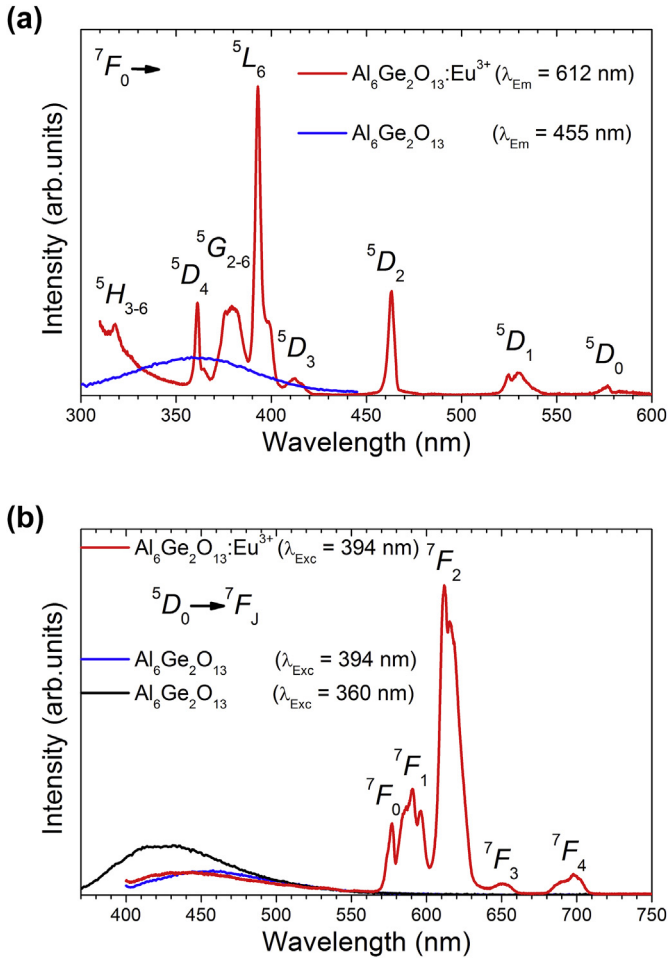

Fig. 6. (a) Excitation photoluminescence spectra of pure and Eu^{3+} doped $Al_6Ge_2O_{13}$ crystalline powders monitoring the emissions at 455 nm and 612 nm, respectively. (b) Emission photoluminescence spectra from pure sample under excitations at 360 nm and 394 nm, and (b) from Eu^{3+} doped sample under excitation at 394 nm.

broad and low intensity emission band centered at 425 nm (violet) when excited at 360 nm, and under excitation at 394 nm the emission band was centered at 455 nm (blue). The origin of this violet-blue emission can be assigned to intrinsic defects in the host such as oxygen vacancies, and interstitial or metal ion (Ge, Al) vacancies, which can coexist. Similar broad band occurs also for Eu^{3+} doped sample; strongly suggesting that is due to intrinsic defects in the $Al_6Ge_2O_{13}$ host. Intrinsic defects are present in the similar structure, the mullite, as mentioned by Schneider et al. [18], probably $Al_6Ge_2O_{13}$ host have the same defect type. Emission from Eu^{3+} doped sample at 612 nm attributed to $^5D_0 \rightarrow {}^7F_2$ transition was observed under excitation at wavelengths between 300 and 600 nm, due to 4f-4f transitions assigned in Fig. 6(a). Under excitation at 394 nm, corresponding to Eu^{3+} $^7F_0 \rightarrow {}^5L_6$ transition, typical Eu^{3+}emission from the $^5D_0$ to $^7F_0$, $^7F_1$, $^7F_2$, $^7F_3$, and $^7F_4$ levels was measured between 570 nm and 710 nm. The most intense peaks are located at 612 nm (red emission-R) and at 590 nm, (orange emission-O) corresponding to the $^5D_0 \rightarrow {}^7F_2$ and $^5D_0 \rightarrow {}^7F_1$ transitions respectively. The intensity relation between red and orange emissions (R/O relation) was 2.7, indicating that the europium ions are distributed in relatively high symmetry sites of the host, and the presence of the emission band at 579 nm assigned to the $^5D_0 \rightarrow {}^7F_0$ attest for the presence in chemical environment without inversion center. In addition, even it was not observed splitting in the $^5D_0 \rightarrow {}^7F_0$ transition, an inhomogeneous broadening suggests a distribution of Eu^{3+} ions in more than one symmetry site into the host. Furthermore, the emission spectra profile considering all $^5D_0 \rightarrow {}^7F_J$ (J = 0, 1, 2, 3, 4) transitions is broadened, which can be attributed to the effect of the distribution of different microenvironment around the Eu^{3+} ion, i.e., distinct symmetry sites occupied by the Eu^{3+} ions in the host, producing inhomogeneous broadening due to the superposition of Stark emission levels. As $Al_6Ge_2O_{13}$ host possess a structure close to that of mullite phase which is constituted by AlO_6 octahedra and AlO_4 tetrahedra sites, can lead us to propose that mostly Eu^{3+} substitutes Al^{3+} in octahedral sites in $Al_6Ge_2O_{13}$ orthorhombic structure.

The $^5D_0$ emission decay curve of the Eu^{3+} ions under excitation at 394 nm, was presented in Fig. 7, and a non-single exponential decay was observed. To estimate the $^5D_0$ excited state lifetime, an averaged lifetime (τ_{ave}) value was calculated by integrating the decay curve using the following equation, and the value obtained was 1.77 ms.

$$\tau_{ave} = \int_{t_0}^{t_f} \frac{I(t)}{I(t_0)} dt \qquad (3)$$

Likewise, the emission decay was fitted by an exponential curve, which the best result was achieved by considering a second order

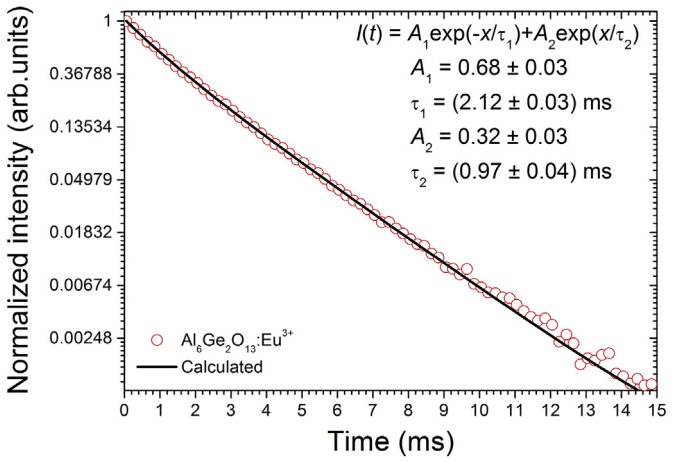

Fig. 7. PL decay curve from the $^5D_0$ level of Eu^{3+} and its bi-exponential fitting.

exponential curve, with lifetime of $\tau_1 = 2.12(3)$ ms and $\tau_1 = 0.97(4)$ ms, and pre-exponential factors $A_1 = 0.68(3)$ and $A_2 = 0.32(3)$, respectively. This result suggests that at least two main species are contributing to the transition. The first one, corresponding to the longer lifetime possibly is due Eu^{3+} ions replacing Al^{3+} sites in the $Al_6Ge_2O_{13}$ crystalline structure, which is coherent with presence of Eu^{3+} in relatively high symmetry site (long as 2.12 ms), probably distorted octahedral site. On the other hand, the fast one can be attributed due to Eu^{3+} on particle surface and/or influenced by OH groups. The hydroxyl groups (-OH) were previously detected by FTIR results. The long component has higher pre-exponential factor than that calculated for the fast one, demonstrating that the higher and isolated Eu^{3+} amounts are distributed into the $Al_6Ge_2O_{13}$ crystalline structure.

As previously presented and discussed by M.H.V. Werts et al. [23] and L.D. Carlos et al. [24] the spontaneous emission probability (A), the radiative lifetime (τ_{Rad}), quantum efficiency for $^5D_0 \rightarrow {}^7F_2$ emission, and Ω_2 and Ω_4 parameters can be calculated, as presented below.

The pure magnetic-dipole character of the $^5D_0 \rightarrow {}^7F_1$ transition enable the determination of intensity parameters from the emission spectrum, because this transition does not depend on the local ligand field experimented by Eu^{3+} ions, that may be used as reference for the entire spectrum [23,24]. The A_{01} spontaneous decay rate of $^5D_0 \rightarrow {}^7F_1$ transition is $A_{01} = A'_{01}n^3$, with $A'_{01} = 14.65$ s^{-1} in vacuum and n is the refractive index of the host. Then, the intensity of the $^5D_0 \rightarrow {}^7F_{0\text{-}6}$ transitions in terms of area of emission curves (S_{0J}) is:

$$S_{0J} = hc\bar{\upsilon}A_{0J}N(5D0), \tag{4}$$

where $N(^5D_0)$ is the $^5D_0$ level population that emits. The total radiative decay rate can be write as:

$$A_T = \sum_{J=0}^{6} A_{0J} = \frac{A_{01}hc\upsilon_{01}}{S_{01}} \sum_{J=0}^{6} \frac{S_{0J}}{hc\upsilon_{0J}} \tag{5}$$

The branching ratio for $^5D_0 \rightarrow {}^7F_{5,6}$ transitions must be neglected due to its low relative intensity, and the radiative contribution can be calculated using only $^5D_0 \rightarrow {}^7F_{0\text{-}4}$ transitions [24].

The emission quantum efficiency (q) is defined by the experimental and radiative lifetimes ratio:

$$q = \frac{\tau_{Exp}}{\tau_{Rad}} \tag{6}$$

The site symmetry and luminescence behavior of Eu^{3+} ions in $Al_6Ge_2O_{13}$ host was carried out by calculations of Judd-Ofelt parameters Ω_λ ($\lambda = 2, 4$). From Judd-Ofelt theory, the intensity parameters Ω_λ are given by:

$$\Omega_\lambda = \frac{3h}{64\pi^4 e^2 \bar{\upsilon}^3} \frac{9}{n(n^2+2)^2} \frac{1}{\left|5D0|U^{(\lambda)}|7FJ\right|^2} A_{0J} \tag{7}$$

The values for reduced matrix elements are 0.0032 of $\lambda = J = 2$ and 0.0023 of $\lambda = J = 4$. Table 2 list the determined values for A_{01}, A_{02}, A_{04}, A_T, τ_{Rad}, q(%), Ω_2 and Ω_4. The emission quantum efficiency was calculated using the three τ_{Exp} values (τ_{av}, τ_1, and τ_2) for comparison. For the calculation, we consider the $n = 1.72$ from Ref. [25] for $Al_6Ge_2O_{13}$ crystalline phase.

The dependence of the radiative lifetime for different hosts originates from the radiation field polarization of the medium and photon density change in an optically dense medium [26]. The oscillator strength of the electric dipole transition for Eu^{3+} and refractive index are considered high in $Al_6Ge_2O_{13}$, then the $^5D_0$ radiative lifetime of Eu^{3+} in $Al_6Ge_2O_{13}$ reduces, i.e., the radiative transition rates are higher, as we can see in Table 2.

In this way, the $^5D_0$ quantum efficiency (q in %) is relatively high, with high values of 64% regarding mostly the Eu^{3+} ions in the crystalline structure. Therefore, when the τ_{ave} is used, the estimated q value is about 54%, and clearly the presence of non-radiative process was considered here. Then we take into account the two experimental lifetimes from decay curve fitted by bi-exponential function, the q values are 64% and 29% for τ_1 and τ_2, respectively, which are due to the Eu^{3+} probably replacing Al^{3+} of AlO_6 octahedra, and Eu^{3+} ions on particle surface and/or influenced by OH groups.

The polarization and asymmetry behavior of the rare-earth ligands are determined by Ω_2 parameter, whereas the other parameter Ω_4 depend on long range effects [27]. The high Ω_2 value for Eu^{3+} in $Al_6Ge_2O_{13}$ host indicate a high asymmetry nature that is corroborated by the R/O ratio (R = Red emission ($^5D_0 \rightarrow {}^7F_2$ transition), and O = orange emission ($^5D_0 \rightarrow {}^7F_1$ transition)) being of 2.7. The low Ω_4 value imply that $^5D_0 \rightarrow {}^7F_2$ transition efficiency increases, or be red colour. Certainly, the $^5D_0 \rightarrow {}^7F_2$ transition is the main emission of Eu^{3+} indicating almost pure red emission in the material.

Table 2
Calculated A_{0J} (J = 1, 2, 4) and A_T radiative decay rates, radiative (τ_{Rad}) experimental (τ_{Exp}) lifetimes, quantum efficiency (q) and Ω_2 and Ω_4 Judd-Ofelt parameters for Eu^{3+} doped $Al_6Ge_2O_{13}$ phase.

Sample	A_{01} (s^{-1})	A_{02} (s^{-1})	A_{04} (s^{-1})	A_T (s^{-1})	τ_{Rad} (ms)	τ_{Exp} (ms)	q (%)	Ω_2 (10^{-20} cm^2)	Ω_4 (10^{-20} cm^2)
1 mol% Eu^{3+} doped $Al_6Ge_2O_{13}$ (This work)	76.65	212.64	12.99	302.29	3.31	1.77 (τ_{ave})	54	4.54	0.40
						2.12 (τ_1)	64		
						0.97 (τ_2)	29		

4. Conclusions

In summary, the results indicated that the samples consisted of well crystallized $Al_6Ge_2O_{13}$ phase in an orthorhombic structure. A simple sol-gel route was used successfully to obtain pure and Eu^{3+} doped $Al_6Ge_2O_{13}$ particles at relative low temperatures, using germanium oxide, aluminum and europium nitrates as metal sources, citric acid as complexing agent, and tetramethylammonium hydroxide, water and ethanol as solvents. The new chemical methodology developed dispenses the use of germanium alcoxydes, which is commonly reported in the literature to prepare compounds based on germanium from chemical procedure. The structural properties of pure and Eu^{3+} doped $Al_6Ge_2O_{13}$ phase is composed by AlO_6, AlO_4 and GeO_4 groups. The materials possess optical bandgap of 4.24 eV and 4.30 eV for pure and Eu^{3+} doped, respectively. The Eu $^{3+}$ doped materials have high PL emission around 612 nm under excitation at 394 nm. The $^5D_0$ level possess two lifetime values: one ~2.12 ms associated to Eu^{3+} replacing Al^{3+} from AlO_6 octahedra of $Al_6Ge_2O_{13}$ crystalline structure and another ~0.97 ms due to Eu^{3+} on particle surface and/or influenced by hydroxyl groups. The quantum efficiency is 64% and 29% for these two Eu^{3+} different sites (two lifetime values), respectively. An average quantum efficiency is 54% considering the average experimental lifetime of 1.77 ms. The Eu^{3+} in $Al_6Ge_2O_{13}$ host have high Ω_2 value that reveal its high asymmetry nature. Finally, good structural and optical emissions of Eu^{3+} doped $Al_6Ge_2O_{13}$ samples were obtained with potential application in displays as red emitters.

Acknowledgments

We acknowledge financial support from the Brazilian Agencies: Conselho Nacional de Desenvolvimento Científico e Tecnológico (CNPq), Instituto Nacional de Ciência e Tecnologia de Fotônica (INCT INFO), Coordenação de Aperfeiçoamento de Pessoal de Nível Superior (CAPES), Fundação de Amparo à Pesquisa do Estado de São Paulo (FAPESP), Fundação de Apoio à Pesquisa da Universidade Federal de Goiás (FUNAPE), and Fundação de Amparo à Pesquisa do Estado de Goiás (FAPEG). Bolsista da CAPES/Estágio Sênior/Processo nº 88881.121134/2016-01.

References

[1] F.M. Faria Filho, R.R. Gonçalves, S.J.L. Ribeiro, L.J.Q. Maia, Mater. Sci. Eng. B 194 (2015) 21.
[2] A. Martucci, G. Brusatin, M. Guglielmi, C. Strohhofer, J. Fick, S. Pelli, J. Sol-Gel Sci. Technol. 13 (1998) 535.
[3] G. Nunzi Conti, S. Berneschi, M. Brenci, S. Pelli, S. Sebastiani, G.C. Righini, C. Tosello, A. Chiasera, M. Ferrari, Appl. Phys. Lett. 89 (2006) 121102.
[4] R. Reisfeld, E. Berman, M. Zelmer, A. Patra, J. Alloys Compd. D. 300–301 (2000) 147.
[5] C. Zhu, A. Monteil, M. El-Jouad, N. Gaumer, S. Chaussedent, Opt. Lett. 34 (2009) 3749.
[6] Y. Yan, A.J. Faber, H. Waal, J. Non-Cryst. Solids 181 (1995) 283.
[7] W.A. Pisarski, J. Pisarski, W. Ryba-Romanowski, Chem. Phys. Lett. 380 (2003) 604.
[8] D. Michel, Ph. Colomban, S. Abolhassani, F. Voyron, Kahn-Harari, J. Eur. Ceram. Soc. 16 (1996) 161.
[9] D. Voll, P. Angerer, A. Beran, H. Schneider, Vib. Spectr. 30 (2002) 237.
[10] R.H. Meinhold, K.J.D. Mackenzie, J. Mater. Chem. 10 (2000) 701.
[11] S. Grandi, P. Mustarelli, S. Agnello, M. Cannas, A. Cannizzo, J. Sol-Gel Sci. Technol. 26 (2003) 915.
[12] J.H. Jang, J. Koo, B.S. Bae, J. Non-Cryst. Solids 259 (1999) 144.
[13] C. Jing, J. Hou, Y. Zhang, J. Phys. D. Appl. Phys. 39 (2006) 1174.
[14] L.J.Q. Maia, R.R. Gonçalves, A.S.L. Gomes, S.J.L. Ribeiro, J. Braz. Chem. Soc. 26 (2) (2015) 2545.
[15] R.M. Soares, A.C.S. Sabioni, I.S. Resck, V.A.S. Falcomer, J.A. Dias, N.M. Silva, S.M.C. Menezes, G.M. Costa, Mater. Res. 10 (2007) 75.
[16] C.O. Paiva Santos, D. Garcia, Y.P. Mascarenhas, J.A. Eiras, Cerâmica 35 (1989) 153.
[17] L. Gao, H. Wang, W.M. Wang, Z.Y. Fu, Chin. J. Inorg. Chem. 23 (2007) 1169.
[18] H. Schneider, R.X. Fischer, J. Schreuer, J. Am. Ceram. Soc. 98 (2015) 2948.
[19] S. Aryal, P. Rulis, W.-Y. Ching, J. Am. Ceram. Soc. 95 (2012) 2075.
[20] R.D. Shannon, Acta Cryst. A 32 (1976) 751.
[21] H.V.S. Pessoni, L.J.Q. Maia, A. Franco Jr., Mater, Sci. Semicond. Proc. 30 (2015) 135.
[22] B. Hapke, Theory of Reflectance and Emittance Spectroscopy, Cambridge University Press, 2012.
[23] M.H.V. Werts, R.T.F. Jukes, J.W. Verhoeven, Phys. Chem. Chem. Phys. 4 (2002) 1542.
[24] L.D. Carlos, R.A. S Ferreira, V. Zea Bermudez, S.J.L. Ribeiro, Adv. Mater 21 (2009) 509.
[25] M.J. Weber (Ed.), Handbook of Optical Materials, CRC Press, 2003.
[26] G. Pan, H. Song, Q. Dai, R. Qin, X. Bai, B. Dong, L. Fan, F. Wang, J. Appl. Phys. 104 (2008) 084910.
[27] S. Som, A.K. Kunti, V. Kumar, V. Kumar, S. Dutta, M. Chowdhury, S.K. Sharma, J.J. Terblans, H.C. Swart, J. Appl. Phys. 115 (2014) 193101.